**Colloid & Polymer Science** Colloid Polym Sci 272:456–466 (1994)

# Fracture behavior of core-shell rubber-modified crosslinkable epoxy thermoplastics

H.-J. Sue, J.L. Bertram, E.I. Garcia-Meitin, J.W. Wilchester, and L.L. Walker

B-1470B, Texas Polymer Center, Dow Chemical USA, Freeport, Texas, USA

*Abstract*: The fracture behavior of a core-shell rubber (CSR) modified crosslinkable epoxy thermoplastic (CET) system, which exhibits high rigidity, high $T_g$, and low crosslink density characteristics, is examined. The toughening mechanisms in this modified CET system are found to be cavitation of the CSR particles, followed by formation of extended shear banding around the advancing crack. With an addition of only 5 wt.% CSR, the modified CET possesses a greater than five-fold increase in fracture toughness ($G_{IC}$), as well as greatly improved fatigue crack propagation resistance properties, with respect to those of the neat resin equivalents. The fracture mechanisms observed under static loading and under fatigue cyclic loading are compared and discussed.

Key words: Rubber modification – low crosslink density high $T_g$ epoxy – toughening mechanisms – double-notch four-point-bend – fatigue fracture

## Introduction

Epoxy resins, possessing adequate chemistries and network structures, can be made ductile under uniaxial or biaxial tension. However, when they are notched and experience a stress triaxiality in front of the notch tip, brittle fracture usually ensues. They need to be toughened.

Toughening of low crosslink density brittle epoxy resins by incorporation of a dispersed rubbery phase has been known to be effective for almost three decades. Typically, an order of magnitude in fracture toughness improvement can be obtained. However, these low crosslink density epoxies usually exhibit rather low ($< 110\,^{\circ}C$) glass transition temperatures ($T_g$) and low creep resistance [1–7]. Therefore, they are only useful for non-structural, low load-bearing types of applications. For aerospace and automotive structural component applications, which often require constant load bearing, only high $T_g$, high modulus, and high creep resistant epoxies can be utilized. Conventional epoxies that possess high $T_g$ often have high crosslink densities. The toughenability of epoxy resins has been clearly shown to be strongly dependent on the crosslink density of the epoxy matrix [4, 5]. Only limited toughening effect can be achieved for highly crosslinked epoxies [4–6]. As a result, there is a strong need to develop a new family of high $T_g$, high rigidity, and low crosslink density epoxies for structural applications.

In an effort to make high $T_g$ and loosely crosslinked epoxies, Bertram et al. [8] and, subsequently, Bauer [9] and Dewhirst [10], and Schultz et al. [11] developed a new family of commercially viable high $T_g$ and low crosslink density epoxies aimed at aerospace structural applications. Their approaches, along with others [12, 13], for making this new family of epoxies are, in fact, quite well-known [1, 2, 4–11]: 1) either stiffer backbone or bulkier side group containing epoxy monomers are synthesized to maintain the high rigidity and high $T_g$ nature of the polymer; 2) either catalyst(s) is used to alter the curing kinetics of the epoxy and/or non-stoichiometric ratio of curing agent is implemented to change the epoxy network structure, which then results in formation of low crosslink density epoxy matrices; 3) high molecular weight rigid monomers are utilized. Consequently, high $T_g$ and low crosslink density and, thus, highly

toughenable epoxies can be readily obtained using the above approaches.

Pearson and Yee convincingly demonstrated that the toughenability of an epoxy matrix is strongly dependent on the crosslink density of the epoxy matrix [4]. They also clearly showed that the roles of the rubber particles in the toughening process are to relieve hydrostatic tension, followed by nucleation of numerous shear bands around the propagating crack [1, 2]. The epoxy matrices they utilized were the diglycidyl ether of bisphenol A (DGEBA) type epoxies; they are not the kind of high performance, highly toughenable epoxies mentioned earlier. Therefore, there is a need to investigate the toughening effect and fracture mechanisms in this new family of rubber-modified high $T_g$, high stiffness, and low crosslink density epoxies. It is important to understand whether or not this new family of epoxies fractures in the same manner as those rubber-modified DGEBA epoxies investigated by Yee and Pearson [1, 2, 4].

The present work focuses on the mechanical behavior investigation of a rubber-toughened crosslinkable epoxy thermoplastic (CET)* system. The CET resin family has a general chemical structure of [14]:

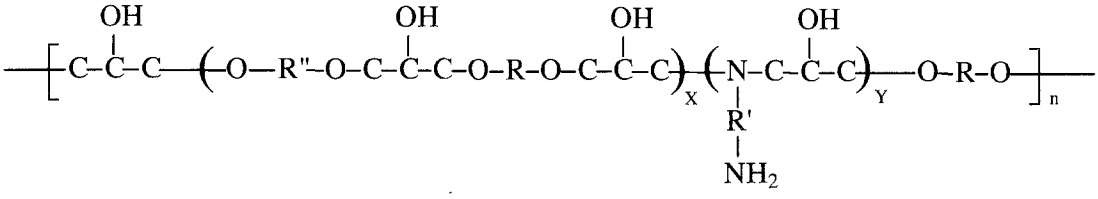

where $X$, $Y$, and $n$ are integers; $R$, $R'$, and $R''$ are the hydrocarbon functional groups [8]. This CET resin family is known to possess very good combined thermal, physical, and processing properties [8, 14]. However, many mechanical property aspects of this resin are still lacking and will be emphasized here. Linear elastic fracture mechanics [15] and various microscopy techniques are employed to conduct mode I (crack opening mode) fracture toughness measurements and the corresponding toughening mechanisms investigations. Dynamic mechanical spectra and fatigue fracture behavior of the neat and core-shell rubber (CSR) modified CET resins are also studied and discussed.

## Experimental

The CET resin and the CSR particle [16] modified CET resin, which had previously been blended with latent catalyst(s) and appropriate curing agent(s) [8], were poured into Teflon-coated glass molds and cured at 150 °C for 4 h, followed by 2 h of post-cure at 200 °C. The CSR-modified CET resin was prepared in a manner similar to that of the CSR-modified DGEBA epoxy system reported earlier [17]. The CSR particle has a butadiene-styrene core (84 weight%) with a styrene-methylmethacrylate-acrylonitrile-glycidyl methacrylate shell (16 weight%) and has a uniform particle size of approximately 120 nm [16, 17]. Five weight percent of CSR particles was added to the CET resin.

The 0.635 cm (0.25″)- and 0.3175 cm (0.125″)-thick CET resin plaques were cast and slowly cooled to room temperature (25 °C) in the oven. The 0.635 cm plaque was machined into bars with dimensions of 12.7 cm × 1.27 cm × 0.635 cm (5″ × 0.5″ × 0.25″) for the double-notch four-point-bend (DN-4PB) [18–20] experiment. Bars with dimensions of 6.35 cm × 1.27 cm × 0.635 cm (2.5″ × 0.5″ × 0.25″) (Fig. 1a) are cut for the single-edge-notch three-point-bend (SEN-3PB) plane strain critical stress intensity factor ($K_{IC}$) fracture toughness measurements [21, 22]. These DN-4PB and SEN-3PB bars were notched with a milling

* The term CET is based on the fact that this family of epoxies can be made with either little or no crosslinking in the cured matrix

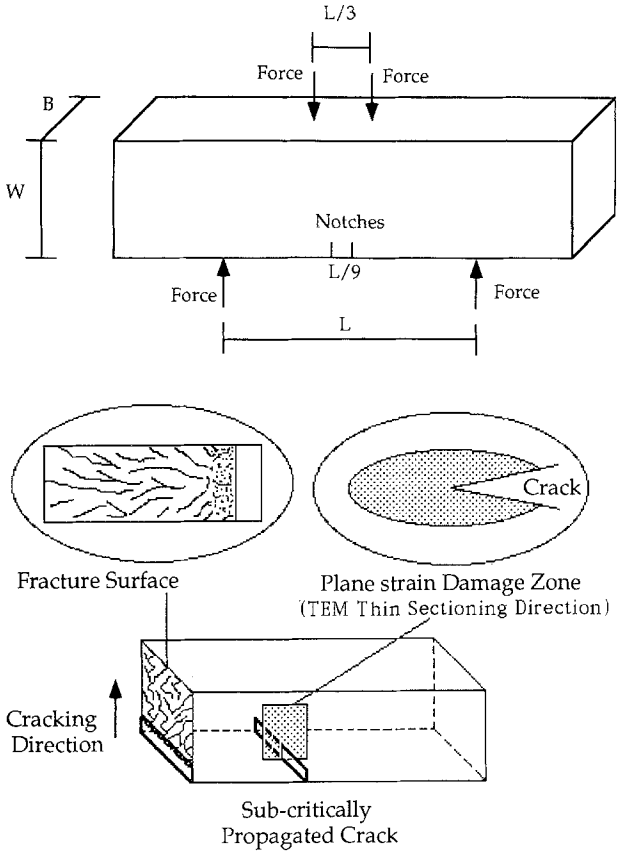


Fig. 1. Schematic of a) DN-4PB specimen and b) the damage zones for transmitted optical microscopy and TEM work. Note that $L = 7.62$ cm, $W = 1.27$ cm, and $B = 0.635$ cm

tool (100 $\mu$m tip radius), followed by razor blade tapping to wedge open a sharp crack with a parabolic crack front. The ratio between the final crack length ($a$) and the specimen width ($W$) was held in the range between 0.4 and 0.6. At least ten SEN-3PB specimens were used for the $K_{IC}$ measurements. The 0.3175 cm CET resin plaque was cut into bars with dimensions of 15.24 cm × 2.54 cm × 0.3175 cm (6″ × 1″ × 0.125″) for SEN tensile fatigue tests [22, 23] and dimensions of 6.35 cm × 1.27 cm × 0.635 cm for both dynamic mechanical spectroscopy and 3PB flexural tests, separately. The sharp notch of the SEN tensile specimen was prepared the same way as that of the SEN-3PB specimens. An $a/W$ ratio of about 0.2 was utilized.

The dynamic mechanical behavior of both the neat resin and the CSR-modified CET was studied using dynamic mechanical spectroscopy (Rheometrics RMS-805) under a torsional mode, with 5 °C per step. A constant strain amplitude of 0.1% and a fixed frequency of 1 Hz were employed. The samples were analyzed at temperatures ranging from − 150 °C to 200 °C. The temperature at which the primary tan $\delta$ peak was located was recorded as $T_g$.

A Sintech-2 screw-driven mechanical testing machine was used to conduct the DN-4PB, the SEN-3PB, and the 3PB flexural experiments. Crosshead speeds of 0.0508 cm/min. (0.02″/min.) and 5.08 cm/min. (2″/min.) were utilized to conduct the SEN-3PB experiment for the neat CET resin and the CSR-modified CET system, respectively. In the DN-4PB experiment, a crosshead speed of 5.08 cm/min. was used for the CSR-modified CET system. Care was taken to ensure that the upper contact loading points were touching the specimen simultaneously. For the 3PB flexural test, a crosshead speed of 0.125 cm/min. (0.05″/min.) was adopted. The flexural modulus was calculated based on the ASTM D790 method.

In the fatigue experiment, a Materials Testing System servo-hydraulic 55 KIP (55 000 lbs) system (Model 810.13) with a MTS 445 controller was used. The fatigue test was performed at 1 Hz with a constant sinusoidal load amplitude and with an $R$-ratio, i.e., minimum load divided by maximum load, of 0.1. The sinusoidal waveform was generated using the MTS Model 436 Control Unit. The linear elastic fracture mechanics method, i.e., $da/dN$ vs. $\Delta K$ (increment of the crack advance/increment of the fatigue cycle vs. difference between the maximum stress intensity factor and the minimum stress intensity factor) approach, was used to characterize the stable fatigue crack propagation region (Paris law region [24]) of the CET resins.

During the fatigue testing, the crack length was constantly monitored using a traveling microscope at about 12 times magnification. The instantaneous crack length and the corresponding fatigue cycles were recorded periodically throughout the test. The $da/dN$ vs. $\Delta K$ curves were obtained as follows. After the $a$–$N$ data were recorded, a fifth power polynomial was fitted to the $a$–$N$ data. The slope of the $a$–$N$ polynomial, i.e., $da/dN$, was then obtained by differentiating the fifth power polynomial. The $\Delta K$ value was

calculated and obtained from the equation below:

$$\Delta K = \frac{\Delta P}{B \cdot W^{0.5}} \cdot Y(a/W) , \quad (1)$$

where $\Delta P$ is the difference between the maximum load and the minimum load, $B$ is the thickness of the specimen, $W$ is the width of the specimen, and $Y$ is the geometric factor, depending on the type of the specimen used and is a function of the crack length ($a$) of the specimen [22]. Since the maximum load, the minimum load, $B$ and $W$ were all known, only the measurement of ($a$) was needed for calculating $\Delta K$. The $da/dN$ vs. $\Delta K$ were then plotted against each other in a log-log format.

The plane strain damage zone around the survived DN-4PB crack was cut normal to the fracture surface, but along the crack propagation direction into two halves using a diamond saw (Fig. 1b). The plane strain core region of these two pieces was prepared for transmitted optical microscopy and transmission electron microscopy (TEM) investigations, respectively.

In the transmitted optical microscopy investigation, a thin, 40-$\mu$m section of the CSR-toughened CET system was obtained by polishing, following the procedure described by Holik et al. [25]. The transmitted optical microscopy thin sections were taken from the mid-section (plane strain region) of the fractured DN-4PB specimens (Fig. 1b). The thin sections were then studied using an Olympus Vanox-S optical microscope both under bright field and cross-polarization condition.

In the TEM microscopy experiment [26], the plane strain core region of the damage zone was carefully trimmed to an appropriate size, i.e., an area of $\approx 5\,\text{mm} \times 5\,\text{mm}$, and embedded in D.E.R.* 331 epoxy resin/diethylene triamine (12:1 ratio by weight). It was cured at 38 °C for 16 h. The cured block was then further trimmed to a size of $\approx 0.3\,\text{mm} \times 0.3\,\text{mm}$ with the crack tip in the damage zone roughly at the center of the trimmed surface. A glass knife was used to face off the trimmed block prior to $OsO_4$ staining. The faced-off block was placed in a vial containing one gram of 99.9% pure $OsO_4$ crystals and stained for 65 h. Ultra-thin sections, ranging from 60 to 80 nm, were obtained using a Reichert–Jung Ultracut E microtome with a diamond knife. The thin sections were placed on 200-mesh formvar-coated copper grid and examined using a JEOL 2000FX ATEM operated at an accelerating voltage of 100 kV for TEM observation.

## Results and discussion

The CET resin family, as pointed out earlier, has very good thermal and physical properties. A resin $T_g$ of up to 200 °C can be obtained using the CET technology [8]. Owing to the low crosslink density network structure of the CET resins, it is believed that the toughenability of these resins should be good. The present work aims at studying the mechanical behavior of the CET and CSR-modified CET systems. It is hoped that, based on this work, better utilization of this type of low crosslink density, high $T_g$, and high stiffness epoxy resins for aerospace structural applications can be achieved.

### *Dynamic mechanical spectroscopy*

The dynamic mechanical spectra of both the neat and the CSR-modified CET resins are shown in Fig. 2. It is evident that the addition of the CSR particles does not affect either the $T_g$ or the plateau modulus of the CET resin. Only the shear storage modulus ($G'$) below $T_g$ is slightly affected by the CSR modification. The rubbery plateau shear modulus ($G_e$) of the CET resin is quite low, i.e., $\approx 3.5$ MPa. This implies that the crosslink density of this system may be low. If the rubber elasticity theory holds for this system and the empirical equation derived by Nielsen [27] and Timm et al. [28] can be applied:

$$\text{Log}_{10} G_e = 6.0 + \frac{293\rho}{M_c} \quad (2)$$

(where $G_e$: rubbery plateau shear modulus, $\rho$: density, and $M_c$: molecular weight between crosslinks), then $M_c$ is approximately equal to 730 g/mole for the CET resin. This suggests that the CET resin indeed has an average $M_c$ value

* Trademark of The Dow Chemical Company

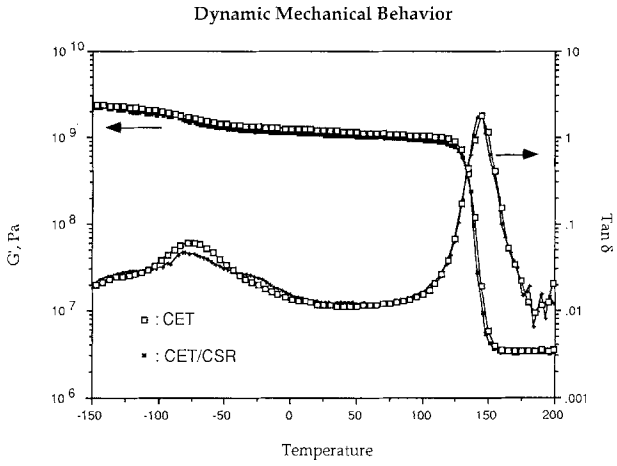


Fig. 2. Dynamic Mechanical Spectroscopy of neat and CSR-modified CET resins

Table 1. Fracture toughness of CET and CSR-modified CET

| Material | $E_{,flex}$ (MPa) | $K_{IC}$ (MPa·m$^{0.5}$) | $G_{IC}$ (J/m$^2$) | $T_g$ (°C) |
|---|---|---|---|---|
| CET | 3250 | 1.00 ± 0.10 | 270 | 144 |
| CET/5% CSR | 3050 | 2.32 ± 0.06 | 1500 | 144 |

higher than that of the DGEBA/piperidine system ($M_c \approx 600$ g/mole, $T_g \approx 95$ °C) [29]. The $T_g$ of the neat and the CSR-modified CET resins are both found to be ≈ 144 °C (Table 1). This is a relatively high $T_g$ resin for having such a low crosslink density.

*Fracture toughness measurement*

The fracture toughness measurements of the CET resins were conducted based on the linear elastic fracture mechanics approach [15, 21]. The equation utilized for calculating the $K_{IC}$ value (Eq. (3)) is similar to Eq. (2):

$$K_{IC} = \frac{P \cdot Y\left(\frac{a}{W}\right)}{B \cdot W^{0.5}}, \quad (3)$$

and the plane strain critical strain energy release rate, $G_{IC}$, can be determined from the following relationship:

$$G_{IC} = \frac{K_{IC}^2 \cdot (1 - \nu^2)}{E}, \quad (4)$$

where $E$ is the Young's modulus and $\nu$ is the Poisson's ratio. In this study, the Young's modulus is assumed to be approximately the same as the flexural modulus and the $\nu$ is assumed to be 0.36 and 0.38 for neat and CSR-modified CET, respectively [30–32].

In order to obtain a linear load-displacement curve during the SEN-3PB experiment, crosshead speeds of 2″/min. (5.08 cm/min.) or higher had to be employed for the CSR-modified CET. While for the neat CET resin system, a crosshead speed of 0.02″/min. (0.0508 cm/min.) was found to be sufficient to generate a linear load-displacement curve. Equations (3) and (4) were utilized to calculate the $K_{IC}$ and $G_{IC}$ values. As shown in Table 1, over five-fold improvement in $G_{IC}$ can be obtained by adding only 5 wt.% of the CSR particles. The toughenability of the CET resin, based on the present study, appears to be as good as that of the DGEBA/piperidine epoxy system [1, 33].

*Investigation of toughening mechanisms*

To study the fracture mechanisms of the CSR-modified CET, it is essential that the damage zone around the subcritically propagated (i.e., nearly fully developed) crack be investigated. Thus, the DN-4PB technique [6, 18–20], which is known to be effective in creating a subcritically propagated crack, is utilized.

The damage feature in this modified system, using the DN-4PB specimen, appears to be similar to that of the CSR-modified polycarbonate [34] as well as that of the dispersed acrylic rubber-modified DGEBA/piperidine system [35, 36]. That is, when the transmitted optical microscopy experiment is conducted, a highly birefringent shear yielded zone, Fig. 3b, is surrounded by a slightly larger dark rubber particle cavitation zone, Fig. 3a. The relative size of the cavitational zone in CSR-modified CET is much smaller than that of the carboxyl terminated copolymers of butadiene-acrylonitrile (CTBN) rubber-modified DGEBA epoxy [37]. As has been discussed by Sue et al. earlier [29, 33], this implies that cavitational resistance of the CSR particles ( ≈ 0.1 μm in size) is probably higher than that of the CTBN rubber particles ( ≈ 2 μm in size). In order to confirm that rubber particle cavitation and matrix shear yielding take place as the crack advances,

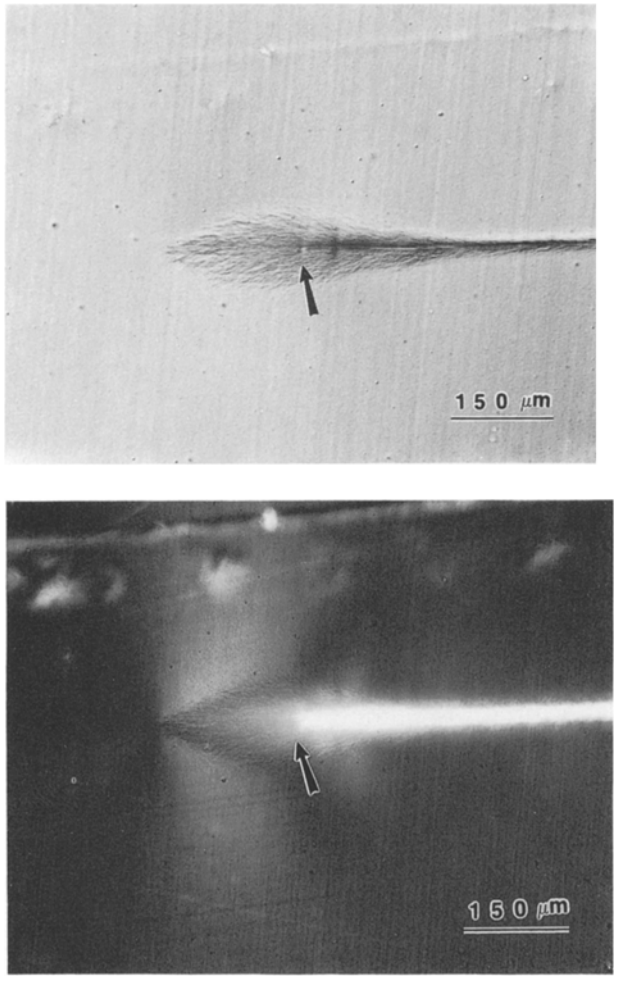


Fig. 3. Transmitted optical micrographs of CSR-modified CET of the DN-4PB damaged crack tip taken under a) bright field and b) cross-polars. This birefringent shear yielded zone (see arrow in b)) is found to be smaller than the dark cavitational zone (see arrow in a))

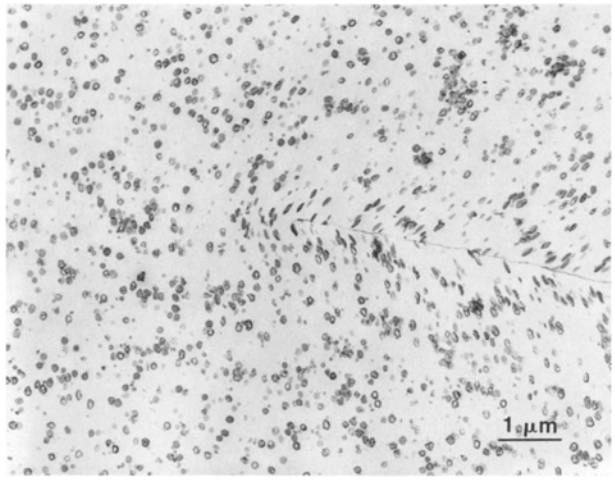


Fig. 4. A TEM micrograph of CSR-modified CET taken at the crack tip of the damaged DN-4PB specimen. About 100% elongation of the CSR particles at the crack tip is found. This indicates that the CET resin is capable of undergoing large scale plastic deformation. The cavity size is found to be smaller outward from the crack tip. The crack propagates from right to left

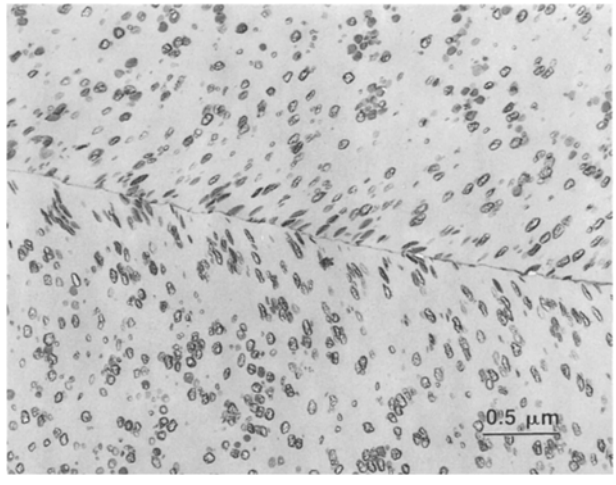


Fig. 5. A TEM micrograph of CSR-modified CET taken in the crack wake of the damaged DN-4PB specimen. The cavity size is found to be smaller outward from the crack wake. The crack propagates from right to left

TEM investigations of the DN-4PB crack tip damage zone were conducted.

As shown in Figs. 4 and 5, when the TEM thin sections of the DN-4PB damage zone are studied, a high degree of CSR particle elongation ( $> 100\%$) is observed around the crack tip and the crack wake. This indicates that at least 100% plastic strain of the matrix has taken place around these highly elongated CSR particles. Farther away from the crack tip and the crack wake, the degree of CSR particle elongation reduces gradually (Fig. 6). The degree of cavitation of the CSR particles (white spots surrounded by dark rubber rings shown in Figs. 4 and 5) is also found to be quite extensive around the crack tip region, and then fades away (Fig. 6) and diminishes at about 100 $\mu$m below the crack (Fig. 7). The size of the CSR cavitation zone observed in TEM is found to be consistent with the transmitted optical microscopy observation made earlier (Fig. 3a).

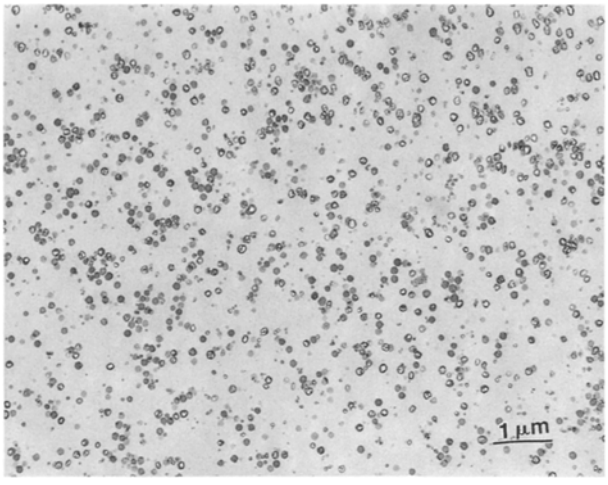


Fig. 6. A TEM micrograph of CSR-modified CET taken about 15 μm below the crack plane, but inside the damage zone. The degree of plastic deformation as well as the size of rubber cavity is decreased away from the crack. The crack propagates from upper right to upper left

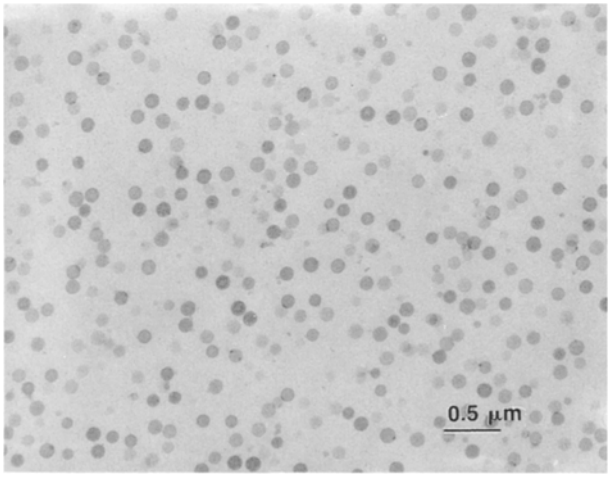


Fig. 7. A TEM micrograph of CSR-modified CET taken about 100 μm away from the crack. The CSR rubber particles appear to be spherical. No cavities are found inside the rubber particles

The toughening mechanisms observed above are in agreement with the previous work conducted by Yee et al. [1–3, 6], suggesting that the roles of the rubber particles in the CET resin toughening process are two-fold: i) relieving the plane strain constraint, followed by ii) nucleation of massive matrix shear bands. The degree of the CSR particle elongation, which is an indication of

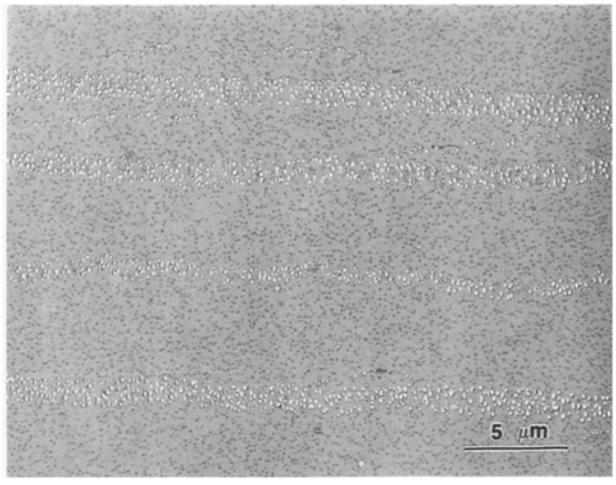


Fig. 8. A TEM micrograph taken in the DN-4PB damage zone of the CSR-modified DGEBA/piperidine system. Highly localized line arrays of cavitated rubber particles are observed

the amount of the surrounding matrix plastic deformation, around the crack tip region in the CET matrix is similar to that in the CSR-modified DGEBA/piperidine system [29, 33]. Although the exact toughening mechanisms and CSR concentrations between the two CSR-modified systems are different, the toughenability of the two resins after CSR modification is quite similar.

The above study reveals that even though the toughenability of the two resins is similar, that even after being modified with the same type of toughener particles, the toughening mechanisms between the two systems can still be very different. This implies that, in addition to the effect due to the crosslink density of the matrix, other physical and mechanical properties, such as, molecular mobility and resistance to shear and dilatational plasticity of the matrix, are also important in affecting the operative toughening mechanism(s). For instance, by comparing the CSR-modified CET and CSR-modified DGEBA/piperidine systems, the later system is more prone to dilatational plasticity. This suggests that the DGEBA/piperidine system network is less resistant to dilatational plasticity than that of the CET system. Consequently, localized line arrays of highly cavitated CSR particles (Fig. 8) are found in the CSR-modified DGEBA/piperidine system [29, 33]. For the CET resin, its resistance to dilatational plasticity should be quite high. No

sign of extensive dilatational plasticity is observed in the CSR-modified CET system (Figs. 4–7).

*Fatigue fracture behavior investigation*

To improve the safety as well as the life-time usage of a functioning structural part requires not only a correct design of the part, but also the use of an appropriate, tough, material to make the part. Adequate knowledge of the fatigue fracture behavior of a material will usually enable design engineers to predict the life-time of a designed part [38]. Therefore, investigations of the fatigue fracture behavior of the neat and toughened CET resins are critical for engineering uses.

*A) da/dN vs. ΔK curve.* Since the traditional *S–N* (stress level vs. number of cycles to failure) fatigue tests are known to be both time consuming and less reproducible at low stress levels [38], the fatigue fracture behavior of both neat CET and CSR-modified CET was investigated using the linear elastic fracture mechanics approach. For comparison purposes, the fatigue fracture behavior of the DGEBA/diaminodiphenylsulfone (DDS) system is also studied. The Log(*da/dN*) vs. Log(*ΔK*) curves of the CET, CSR-modified CET and DGEBA/DDS systems in the Paris' law region [39] are plotted in Fig. 9. Owing to the experimental complexity, the $\Delta K_{\text{threshold}}$ portion of the curve was not measured [38].

As indicated in Fig. 9, even though the CET resin is quite ductile under uniaxial tension [14], the fatigue fracture behavior of the CET resin is not much better than that of the DGEBA/DDS system. In other words, without toughening, brittle fatigue fracture ensues. Toughening of the CET resin under fatigue loading conditions is thus needed.

With only 5 wt.% CSR modification, a significant improvement of the fatigue performance is observed in CET. That is, the curve shifts to the far right of the plot with a slight reduction of the slope from 4.6 to 3.7. In other words, a much higher *ΔK* is now required to propagate the crack in the CSR-modified CET system at the same rate as in the neat CET system. The significant fatigue performance improvement in the toughened CET is mainly due to the presence of the CSR particles. In an effort to understand how the CSR particles help improve the fatigue resistance of the CET

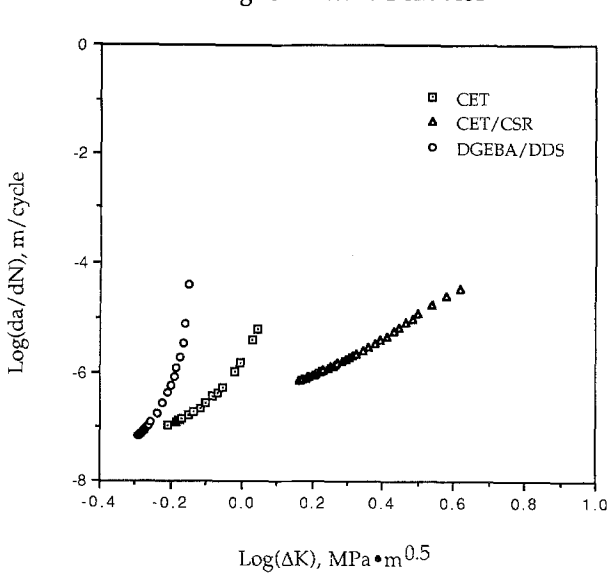


Fig. 9. Log(*da/dN*) vs. Log(*ΔK*) plots of the CET, CSR-modified CET, and DGEBA/DDS epoxy systems. The curves that locate at the lower right are more fatigue resistant. Therefore, the CSR-modified CET exhibits the best fatigue performance, followed by CET, and by DGEBA/DDS, under the specified fatigue loading condition

resin, the damage zone of the fatigued CSR-modified CET is investigated using both transmitted optical microscopy and TEM.

*B) Toughening mechanisms under fatigue crack growth.* The damage zone of a partially grown fatigue crack (stopped at $\Delta K \approx 1.8\ \text{MPa}\cdot\text{m}^{0.5}$) was analyzed using both transmitted optical microscopy and TEM. The transmitted optical micrographs of the damage zone under fatigue loading resemble that of the static crack growth condition (Fig. 3). They will not be shown here. When the TEM investigation is conducted, the toughening mechanisms in the CSR-modified CET are, in general, similar to those observed in the static loading case. That is, the rubber particles help to dissipate the crack tip bulk strain energy, which is followed by promotion of numerous shear bands. In addition, the fatigue loading causes the crack path to become much more tortuous (Figs. 10 and 11). That is, the crack deflection mechanism is more prominent under fatigue loading [40, 41]. No evidence of rubber particle debonding is found. Furthermore, under fatigue loading, there appears to be a noticeably more

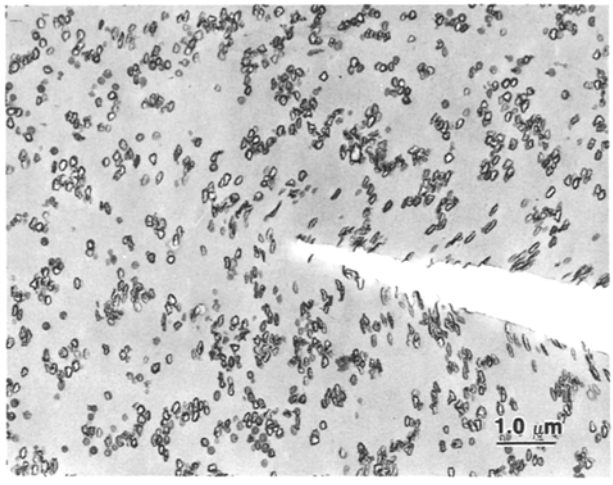


Fig. 10. A TEM micrograph of CSR-modified CET taken at the crack tip after fatigue loading (stopped at $\Delta K \approx 1.8\ \mathrm{MPa \cdot m^{0.5}}$). The toughening mechanisms under fatigue loading is similar to those under static loading shown in Fig. 4, except that a much more tortuous crack path is observed here

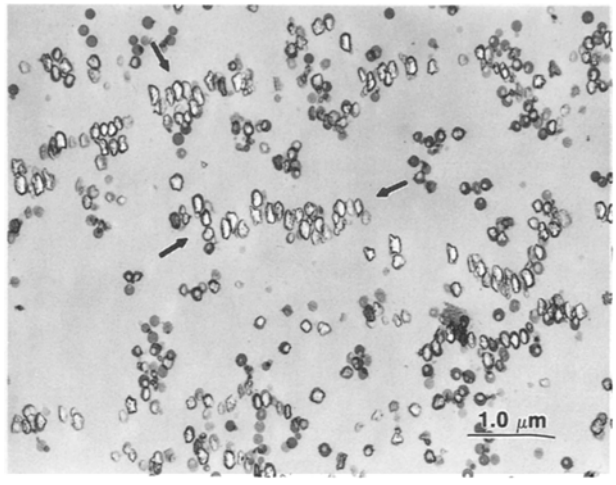


Fig. 12. A TEM micrograph of CSR-modified CET taken about 5 $\mu$m below the crack plane, but inside the damage zone, after fatigue loading (stopped at $\Delta K \approx 1.8\ \mathrm{MPa \cdot m^{0.5}}$). Highly localized damage pattern is observed (see arrows)

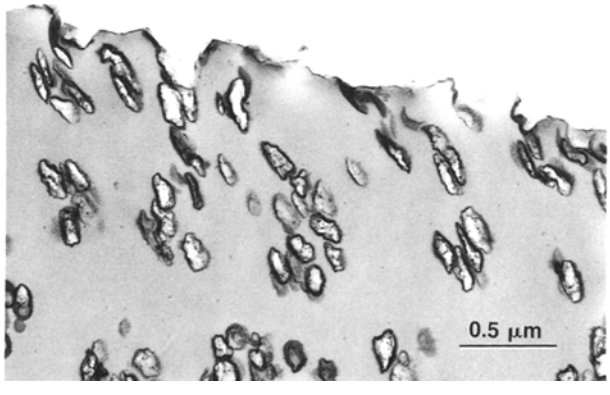


Fig. 11. A TEM micrograph of CSR-modified CET taken in the crack wake after fatigue loading (stopped at $\Delta K \approx 1.8\ \mathrm{MPa \cdot m^{0.5}}$). A tortuous crack path is observed

highly localized damage pattern inside the damage zone (see arrows in Fig. 12), in comparison with that of the static loading condition. In other words, the damage pattern in fatigue loading is not as progressive as that in the static loading case, where the degree of dilatational and shear plasticities is most severe adjacent to the crack and gradually diminishes away from the crack. The formation of the highly localized fatigue damage pattern may be due to the local variation of dispersion of CSR particles in the matrix around the crack. The local variation of morphological differences in the matrix around the propagating crack is known to have more effect on crack path for fatigue loading than that for static loading.

It is known that the loading frequency, types of cyclic loading, mean stress level, and $R$-ratio will all affect fatigue performance [38], and therefore, the operative toughening mechanisms. Hence, the operative toughening mechanisms under other types of fatigue loading conditions may not be the same as the toughening mechanisms described and discussed above. They are the subject of future investigations.

The physics of the rubber particle cavitational process are very complex. The rubber particles, before being mechanically loaded, can experience a high magnitude of hydrostatic tension, resulting from thermal stress build-up [42]. However, cavitation of the rubber particles usually does not occur as long as the bonding between the rubber particle and the matrix is adequate and the cohesive strength of the rubber particles is reasonably strong [1, 2, 4, 17, 29, 33]. When the already thermally stressed rubber particles are stressed in front of a sharp crack tip, an extremely high level of stress triaxiality is established. This high level of

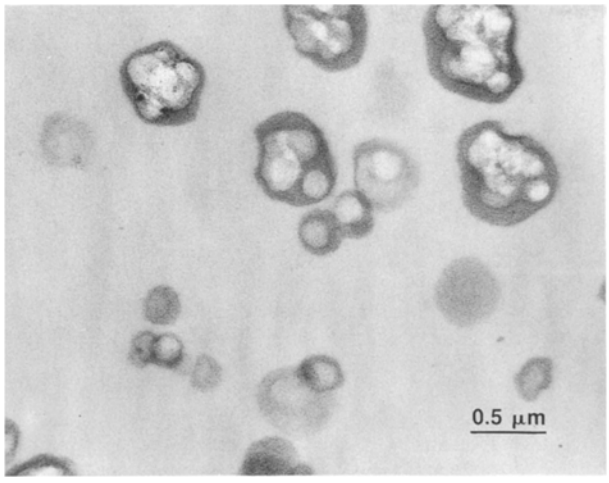


Fig. 13. A TEM micrograph of CSR-modified CET taken inside the DN-4PB damage zone. The cavities inside the cavitated rubber particles are spherical in nature

stress triaxiality can cause the rubber particles to cavitate and results in the redistribution of the stress field around the cavitated rubber particles [43]. Consequently, the surrounding matrix, instead of experiencing a highly triaxial stress state, experiences a build-up of the octahedral shear stress component. This build-up of the octahedral shear stress component promotes large scale shear banding in the matrix [44].

It is noted that the numbers of cavities inside the cavitated rubber particles can be more than one (Fig. 13). Some of the cavities inside the cavitated rubber particles appear to be connected with either fibrils or thin films, or both. Some cavities, however, appear to be empty. The majority of these cavities appear to be spherical in shape. This implies that the fracture phenomenon inside the rubber particles is forming holes, instead of sharp line cracks as in the case for rigid polymers. When the magnitude of the hydrostatic tension becomes larger, the size of the holes also increases [1, 2, 4, 17, 29, 33].

It is also noticed that the apparent volume fraction of the CSR particles in the CET matrix shown in Figs. 4–7 is higher than the actual volume fraction of the rubber utilized (10% vs. 7% by volume). This is because the thickness of the TEM thin section is comparable to the diameter of the CSR particle ( $\approx 0.1$ $\mu$m). This results in a projection of three dimensional images into a two dimensional image during the TEM imaging (Figs. 4–7). Therefore, care has to be taken when quantitative correlation between morphology and fracture mechanisms of rubber-modified polymeric systems are to be made using TEM micrographs.

## Conclusion

The fracture behavior of the neat and CSR-modified CET resins were studied. The toughening effect, under both monotonic and cyclic loading conditions, is found to be quite impressive. The toughening mechanisms observed in the CSR-modified system are mainly due to rubber particle cavitation, which relieves the triaxial tension in front of the crack tip, followed by the formation of shear bands. The toughenability of the CET resin, based on the present study, appears to be as good as that of the DGEBA/piperidine epoxy system.

*Acknowledgement*

The authors would like to thank C.E. Allen, N.A. Orchard, W.L. Huang, P.M. Puckett, D.L. Barron, B.L. Burton, D.M. Pickelman, C.J. Bott, C.C. Garrison, J.D. Earls, H.-P. Chen, R.E. Hefner, R.D. Peffley, J.L. Potter, and T.M. Fisk, for their support, discussion, and material supplied for this work.

*Notice*

The information in this paper is presented in good faith, but no warranty, express or implied, is given, nor is freedom from any patent to be inferred.

### References

1. Yee AF, Pearson RA (1986) J Mater Sci 21:2462
2. Pearson RA, Yee AF (1986) J Mater Sci 21:2475
3. Lee H, Neville K (1967) Handbook of Epoxy Resins. McGraw-Hill, New York
4. Pearson RA, Yee AF (1989) J Mater Sci 24:2571
5. Bradley WL, Schultz W, Corleto C, Komatsu S (1993) Chap. 3 in Toughened Plastics I – Science and Engineering. Riew CK, Kinloch AJ (eds) Adv Chem Ser, 233, Amer Chem Soc, Washington, DC, p 317
6. Sue H-J (1991) Polym Eng Sci 31:275
7. Kinloch, AJ (1989) Chap 3 in Rubber-Toughened Plastics. Riew CK (ed) Adv Chem Ser, 222, Amer Chem Soc, Washington, DC, p 67
8. Bertram JL, Walker LL, Berman JR, Clarke JA (1986) US Patent 4,594,291
9. Bauer R (1986) 18th International SAMPE Tech Conf, Oct 7–9
10. Dewhirst KC (1988) Us Patent 4,786,668

11. Schultz WL, Portelli GB, Jordan RC, Thompson WL (1988) Polym Preprint 29:136
12. Bishop MT, Bruza KJ, Laman SA, Lee WM, Woo EP (1992) ACS Polymer Preprints 33(1):362
13. Covavisaruch S, Robertson RE, Filisko FE (1992) J Mater Sci 27:990
14. Burton BL, Swartz CA (1987) PMSE, Amer Chem Soc 57:201
15. Williams JG (1984) Fracture Mechanics of Polymers. John Wiley & Sons, New York
16. Henton DE, Pickelman DM, Arends CB, Meyer VE (1988) US Patent 4,778,851
17. Sue H-J, Garcia-Meitin EI, Pickelman DM, Yang PC (1993) Chap 10 in Toughened Plastics I – Science and Engineering. Riew CK, Kinloch AJ (eds) Adv Chem Ser, 233, Amer Chem Soc, Washington, DC, p 259
18. Sue HJ, Pearson RA, Parker DS, Huang J, Yee AF (1988) Polym Preprint 29:147
19. Sue H-J (1991) Polym Eng Sci 31:270
20. Sue H-J, Yee AF, J. Mater Sci 28:2975
21. ASTM Standard, E399-90
22. Towers OL (1981) Stress Intensity Factor, Compliance. and Elastic $\eta$ Factors for Six Geometries. The Welding Institute, Cambridge, England.
23. ASTM Standard, E647-90
24. Paris PC (1964) Fatigue – An Interdisciplinary Approach. Proceedings 10th Sagamore Conf, Syracuse Univ Press, Syracuse, New York
25. Holik AS, Kambour RP, Hobbs SY, Fink DG (1979) Microstruct Sci 7:357
26. Sue H-J, Garcia-Meitin EI, Burton BL, Garrison CC (1991) J Polym Sci, Polym Phys Ed 29:1623
27. Nielsen LEJ (1969) J Macromol Sci C3:69
28. Timm DC, Ayodeji AJ, Foral RF (1985) Br Polym J 17:227
29. Sue H-J (1992) J Mater Sci 27:3098
30. Moloney AC, Kausch HH, Kaiser T, Beer HR (1987) J Mater Sci 22:381
31. Huang Y, Kinloch AJ (1992) J Mater Sci 27:2763
32. Huang Y, Kinloch AJ (1992) J Mater Sci Letters 11:484
33. Sue H-J, Garcia-Meitin EI, Orchard NA (1993) J Polym Sci, Polym Phys Ed 31:595
34. Parker DS, Sue HJ, Huang J, Yee AF (1990) Polymer 31:2267
35. Sue H-J, Hoffman DW, unpublished work
36. Hoffman DK, Arends CB (1987) US Patent 4,708,996
37. Pearson RA, Yee AF (1991) J Mater Sci 26:3828
38. Hertzberg RW, Manson JA (1980) 'Fatigue of Engineering Plastics. Academic Press, New York
39. Paris PC (1964) Fatigue – An Interdisciplinary Approach, Proceedings 10th Sagamore Conf, Syracuse Univ Press, Syracuse, New York
40. Karger-Kocsis J, Friedrich K (1992) Colloid Polym Sci 270:549
41. Ritchie RO, Yu W (1986) Short Crack Effects In Fatigue: A Consequence Of Crack Tip Shielding in Small Fatigue Cracks. Ritchie RO, Lankford J (eds) TMS-AIME, Warrendale, PA
42. Boyce ME, Argon S, Parks DM (1987) Polymer 28:1680
43. Sue H-J (1988) Mechanical Modeling and Experimental Observations of Toughened Rigid-Rigid Polymer Alloys. Ph D Thesis, The University of Michigan, Ann Arbor
44. Yee AF (1986) Modifying Matrix Materials for Tougher Composites in "Toughened Composites" STP 937, Johnston NJ (ed) ASTM, Philadelphia, 383

Received January 12, 1993;
accepted May 7, 1993

Authors' address:

Dr. H.-J. Sue
B-1470B, Texas Polymer Center
Dow Chemical USA
Freeport, Texas 77541, USA